

## Synthesis and magnetic characterization of $\text{LaMnO}_3$ nanoparticles

E. Hernández<sup>a</sup>, V. Sagredo<sup>a</sup> and G.E. Delgado<sup>b</sup>

<sup>a</sup>Laboratorio de Magnetismo, Departamento de Física, Facultad de Ciencias,  
Universidad de Los Andes, Mérida 5101, Venezuela.

<sup>b</sup>Laboratorio de Cristalografía, Departamento de Química, Facultad de Ciencias,  
Universidad de Los Andes, Mérida 5101, Venezuela.

Received 26 November 2014; accepted 30 January 2015

$\text{LaMnO}_3$  Nanoparticles systems were prepared by the sol-gel auto-combustion method, in order to analyze the structure and magnetic behavior presented by the compound prepared following a new alternative route of synthesis. Structural characterization, morphology and crystallite size was performed by X-ray diffraction (XRD), infrared spectroscopy (IR) and electron microscopy (TEM). The XRD study together with a Rietveld analysis showed that the  $\text{LaMnO}_3$  compound crystallized in a perovskite hexagonal structure. The IR spectra showed that the compound has tensile energy bands in the Mn-O-Mn bonds related with the octahedron  $\text{MnO}_6$ ; which are attributed to a characteristic vibration of the  $\text{ABO}_3$  perovskite. An estimated size and morphological analysis was carried out by applying the Scherrer's formula and using Transmission Electron Microscopy (TEM), revealing non-spherical shape and particle sizes between 13 nm and 18 nm. The magnetic measurements  $M(T)$  were performed by using zero-field-cooled (ZFC) and field-cooled (FC) protocols which revealed a positive Weiss temperature indicating the presence of ferromagnetic interactions with a Curie temperature,  $T_C = 150$  K.

**Keywords:** Auto-combustion; curie temperature; magnetization; manganites; nanoparticles; ferromagnetism; perovskite; Sol-Gel.

PACS: 75.60.Ej; 75.47.Lx; 73.22.-f; 81.20.Fw

### 1. Introduction

Manganites are mixed oxides of manganese which crystallizes in perovskite structure, and whose broad stoichiometric formula is  $\text{ABO}_{(3\pm\delta)}$ ; where A is a lanthanide element and B is manganese, which also includes the ability to generate an exact or not oxygen stoichiometry. One of the highlight characteristics of manganites perovskites compared with other families of oxides is the wide variety of substitutions that may accept its crystal structure. The lanthanides are among the examples of about 25 elements which can occupy the position; on the other hand, apart from the manganese almost 50 different elements are able to occupy the B site [1,2]. Usually the manganite compounds crystallize in structure  $\text{ABO}_3$  perovskites; in which it is possible to have an ideal cubic structure of  $\text{P}_{m\bar{3}m}$  space group, orthorhombic  $\text{P}_{bnm}$  space group or rhombohedral  $\text{R}_{3\text{CH}}$  space group. The stoichiometry with the corresponding valence states to Manganite is  $\text{A}^{+3}\text{B}^{+3}\text{O}_3^{-2}$ , assigning a cubic unit cell body centered, bcc, in whose center stands the  $\text{A}^{+3}$  cation that is usually the largest one;  $\text{B}^{+3}$  cations occupy the eight apex of the cell and  $\text{O}^{-2}$  anions occupy the midpoints between cations, in the middle of the edges of the bcc cell, as illustrated in Fig. 1 [3-5].

### 2. Synthesis

$\text{LaMnO}_3$  nanoparticles were synthesized by the sol-gel auto-combustion method, this is an attractive synthetic route and has been used to prepare a variety of nanoferrites compounds [6-8]. The precursors used were Manganese(II) nitrate,  $\text{Mn}(\text{NO}_3)_2 \cdot 4\text{H}_2\text{O}$  and lanthanum oxide,  $\text{La}_2\text{O}_3$ . Stoichiometric amounts of manganese nitrate were dissolved in distilled water, stirring for 10 minutes at room temperature.

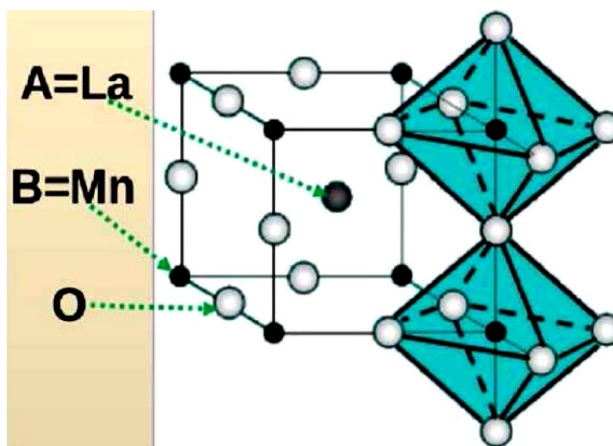
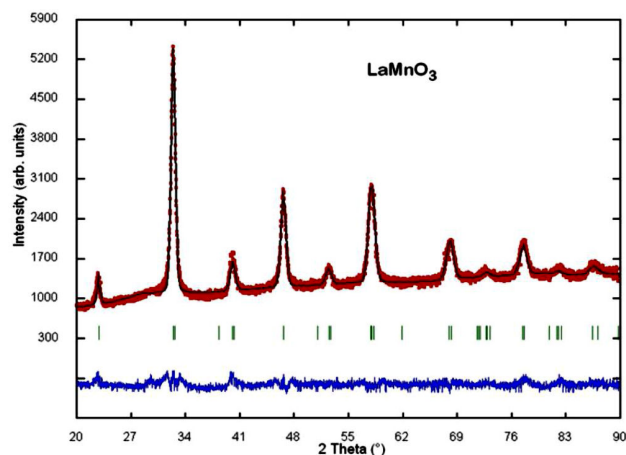


FIGURE 1. Ideal cubic perovskite  $\text{LaMnO}_3$ .

As the source of lanthanum was its oxide, it was necessary to dissolve it in nitric acid,  $\text{HNO}_3$  and distilled water in an stoichiometric amount needed to get 2gr of  $\text{LaMnO}_3$ ; maintaining the whole mixture under stirring for 20 minutes at temperature  $65^\circ\text{C}$ ; thus lanthanum nitrate,  $\text{La}(\text{NO}_3)_3$ , was achieved. On the other hand, citric acid,  $\text{C}_6\text{H}_8\text{O}_7 \cdot \text{H}_2\text{O}$  was used as organic fuel with a combustion heat of  $H_C=18.3$  KJ, which is easily dissolved in distilled water stirring at room temperature for 10 minutes. All the solutions were prepared separately until getting a completely clear solution; then they were mixed and kept under stirring in a beaker on a hotplate at  $85^\circ\text{C}$  for 4 hours until the final product had a viscous and yellow appearance. After this, the sol-gel obtained was placed in a shuttle glass and inserted in the center of a tubular furnace preheated to  $500^\circ\text{C}$ , which is slightly inclined to get a slight convection allowing air circulation at the time when the



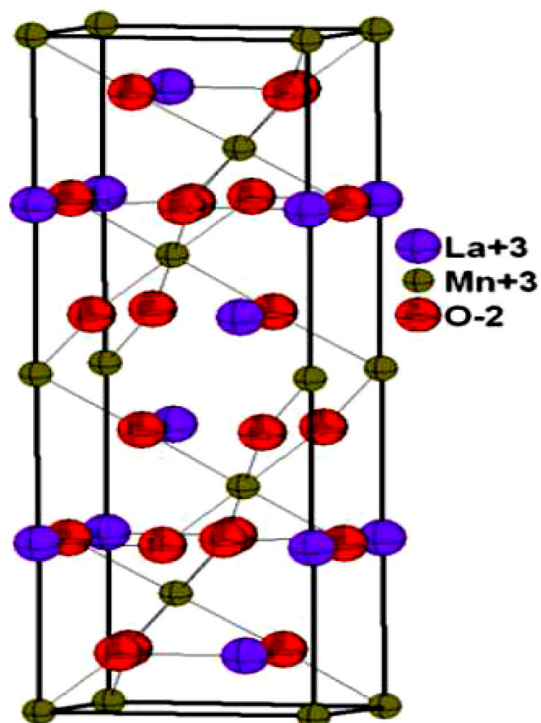
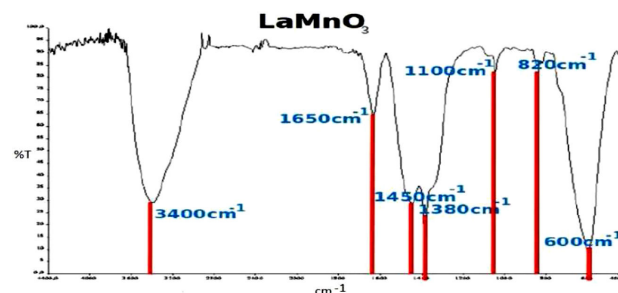
FIGURE 2. Tubular furnace.

FIGURE 3. Rietveld refinement plot for LaMnO<sub>3</sub>.

combustion occurred, the tubular furnace is shown in Fig. 2. After a few seconds of entering the sol-gel in the oven a violent appearance of flames shows that the process of self-combustion occurred, releasing large amounts of gases. Just after about 3 minutes the material stops emitting gases, the oven was turned off and allowed to cool down to room temperature. It is noted that the obtained material is spongy and grayish. The material was removed from shuttle glass (when the combustion occurred part of the material leaved the shuttle glass; but it was discarded, only the material which remain inside the shuttle glass after combustion was used in the characterizations) and ground it gently in a agate stone, thus the LaMnO<sub>3</sub> nanoparticles were obtained.

### 3. Results and Discussion

The LaMnO<sub>3</sub> nanoparticles were characterized by X-ray diffraction at room temperature without further treatment. The crystal structure and unit cell parameters have been evaluated by Rietveld refinement using Fullprof suite program. This procedure allowed us to determine that the compound crystallized as a hexagonal perovskite structure with space

FIGURE 4. Unit cell diagram for LaMnO<sub>3</sub>.FIGURE 5. FT-IR spectra for LaMnO<sub>3</sub>.TABLE I. Rietveld refinement results for LaMnO<sub>3</sub>.

Atom	Ox	site	<i>x</i>	<i>y</i>	<i>z</i>	foc
La	+3	6a	0	0	0.25	1
Mn	+3	6b	0	0	0	1
O	-2	18e	0.459(5)	0	0.25	1

group  $R_{-3C}$  and unit cell parameters  $a = 5,5176(4)$  Å and  $c = 1,425(3)$  Å.

Figure 3 shows the Rietveld fit to the XRD data taken for LaMnO<sub>3</sub>. Table I shows the Rietveld refinement results in the hexagonal space  $R_{-3C}$  group. The crystallites sizes were calculated by using Scherrer's formula for the plane (110) [21], the obtained values lies in the range 5-27 nm for nanoparticles with average value of 15 nm. From the information provided by Rietveld adjustment and crystallographic tabs, mentioned above, make to suspect that the LaMnO<sub>3</sub> compound

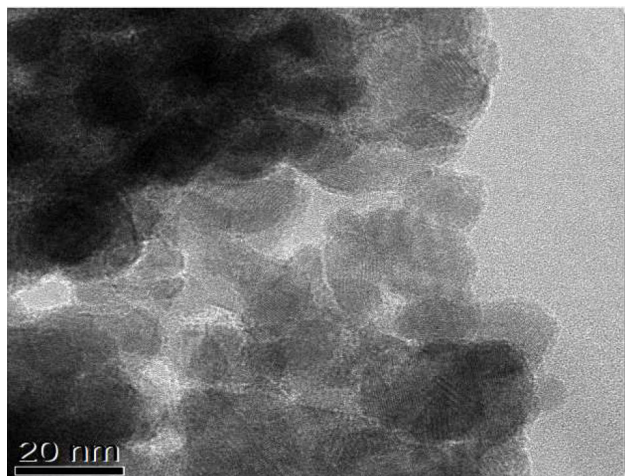


FIGURE 6. TEM micrographs of LaMnO<sub>3</sub> nanoparticles.

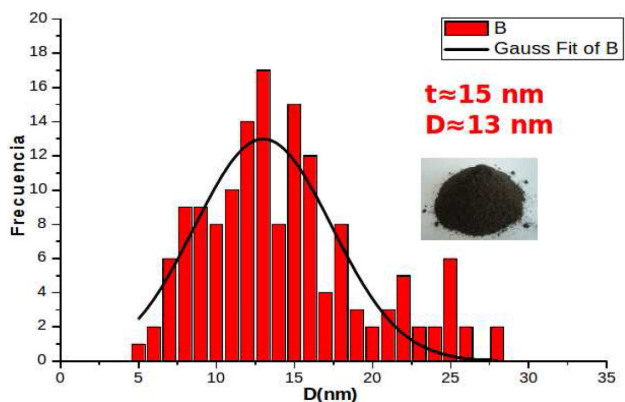


FIGURE 7. Size distribution for the LaMnO<sub>3</sub> sample.

crystallized in a structure that presumably do not keep inexact stoichiometry in oxygen, LaMnO<sub>3±δ</sub>. When the compound retains an exact stoichiometry in oxygen, this usually crystallizes in orthorhombic perovskite structure [8,9]. The structure found here is a hexagonal perovskite which corresponds to a structure with characteristics between cubic and orthorhombic.

Figure 5 shows the FI-IR spectrum for LaMnO<sub>3</sub> nanoparticles. This shows that the most significant absorption bands are located around 600, 820, 1100, 1380, 1450 1650 and 3400 cm<sup>-1</sup>. The absorption band at 600 cm<sup>-1</sup> corresponds to the stretching mode, linked to the internal movement of a length change of the bounds Mn-O-Mn associated with the octahedron MnO<sub>6</sub> attributed to a vibration characteristic of the perovskite type ABO<sub>3</sub> [10,11]. This result is in good agreement with the analysis of X-ray diffraction. The bands in the region around 3400 cm<sup>-1</sup> correspond to O-H and La(OH) bonds. The water present in the samples may result to the hygroscopic condition of the compounds. The bands around 1650 cm<sup>-1</sup> are assumed to correspond at bending vibrations of the N-H bonds (secondary amines); the bands around 1380 and 1450 cm<sup>-1</sup> are produced by bending vibrations in the bonds N-O (nitrates). In 1100 and 820 cm<sup>-1</sup>

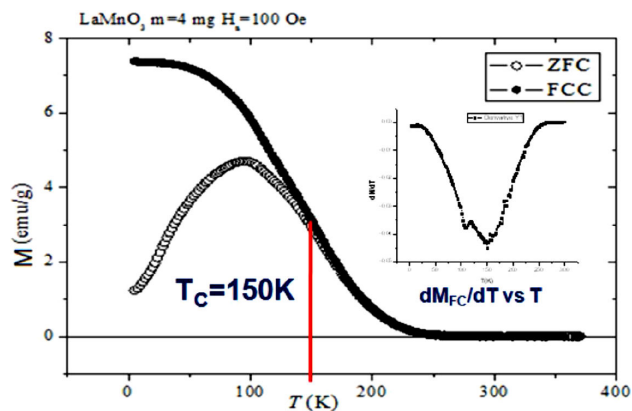


FIGURE 8. Temperature dependence of the magnetization on nanoparticles of LaMnO<sub>3</sub>; *M* vs *T*.

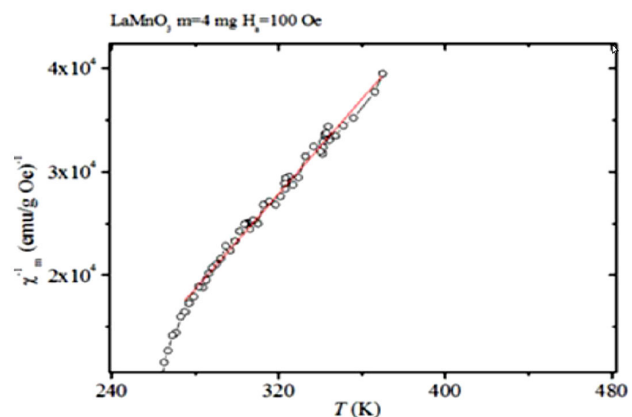


FIGURE 9. LaMnO<sub>3</sub> 1/χ vs T; θ<sub>w</sub> = 190 K.

are C-O vibrations bonds (Carbon) which may correspond to residues due to the sol-gel auto-combustion method [12-14].

Figure 6 shows an image of LaMnO<sub>3</sub> nanoparticles taken with a transmission electron microscope with 20 nm full scale. In this micrograph it can be observed that the nanoparticles have an undefined shape and there is a size distribution (In spite of micrograph quality we did take the necessary information). This result is related to the synthesis method, since the self-combustion is not performed in the total thermal equilibrium of the temperature in different parts of the sample, Therefore the flame appears at different time, so this effect may cause a distribution of grain sizes of the obtained nanomaterial.

Figure 7 shows the graph of particle diameter versus frequency obtained from the LaMnO<sub>3</sub> micrograph of which was fitted with a Gaussian bell-type displays. This allowed us to estimate an average particle size of *D* = 13 nm. In order to obtain this size distribution was necessary to measure on the micrograph the diameter of about 120 particles. The statistical data were taken by hand using a scale ruler which brings the IMAQ-Vision Builder program that comes with the micrographs own. As the particles shape are not spherical, several measurement on each particle (diameters between 4 and 5) were made to have a simple average for each particle diameter.

In Fig. 8 is shown the temperature dependence of the DC magnetization measured at magnetic field of 100 Oe between 5 K and 380 K which follow the FC and ZFC protocols for nanoparticles of LaMnO<sub>3</sub>. The curve  $M_{FC}(T)$  presents a typical paramagnetic to ferromagnetic transition. In order to get the transition temperature we draw  $dM_{FC}(T)/dT$  vs  $T$ , presented in the insert of Fig. 8. The obtained Curie temperature was  $T_C = 150$  K from the minimum of the drawing. It is noted that the ZFC curve presents a maximum located at  $T_{Mas-ZFC} = 98$  K, the sharp decrease of the magnetization ZFC below the peak indicates the likelihood of the presence of antiferromagnetic interactions in the compound [22].

Figure 9 shows the graph  $1/\chi$  make with the data  $M_{FC}$  vs  $T$  in the paramagnetic region from 270 K to 380 K. The extrapolation of the linear fit to the  $T$  horizontal axis, according to the Curie-Weiss law, yield the value of the Weiss temperature,  $\theta_w = 190$  K. The positive sign of this temperature suggests that the predominant interactions between the magnetic atoms are ferromagnetic which was established by the Curie temperature obtained above.

#### 4. Conclusions

From the results, it is suggested that LaMnO<sub>3</sub> nanoparticles synthesized by sol-gel auto-combustion method exhibit a ferromagnetic behavior; which has been reported in some previous studies [15-18]. These result suggest that there is no exact stoichiometry in oxygen; that is, a compound of type LaMnO<sub>(3±δ)</sub>. If that is the case, the Mn<sup>+3</sup>-O<sup>-2</sup>-Mn<sup>+3</sup> in the MnO<sub>6</sub> octahedron do not occur correctly because the va-

cancies in oxygen and/or manganese does not support the super-exchange magnetic interaction which is what would happen if the stoichiometry is exact. This is associated with an antiferromagnetic magnetic interaction. Consequently, the presence of oxygen vacancies and/or manganese due to non-stoichiometry in the ferromagnetic compound support ferromagnetic interactions and not the antiferromagnetic one that is reported in some literature [10]. However, it is probable, that in this case the samples obtained have the composition La<sup>+3</sup>Mn<sup>+3</sup><sub>(1±α±β)</sub>Mn<sup>+4</sup><sub>(α)</sub>Mn<sup>+2</sup><sub>(β)</sub>O<sup>-2</sup><sub>(3±δ)</sub> [15] whose predominance of the double exchange magnetic interaction as it will link the type Mn<sup>+4</sup>-O<sup>-2</sup>-Mn<sup>+3</sup> and Mn<sup>+3</sup>-O<sup>-2</sup>-Mn<sup>+2</sup>. All of the above comments would be factors affecting the value of the effective magnetic moment of the sample under study. It is assumed that in this case, no accuracy in the oxygen stoichiometry is due to inherently synthesis process since in the combustion stage there was not enough proportion of oxygen necessary for the combustion process producing a shift of the stoichiometry in oxygen. However there are reports of a non-stoichiometric for lanthanum manganite because they are highly oxidizable [19-21].

#### Acknowledgments

The authors want to acknowledge to the CDCHTA-ULA for funding the proyect C-1658-09-05-A.

The authors want to acknowledge to C. Pernechele and F. Rossi. Dipartamenti di Fisica, CNISM, Universita di Parma, A-1-43100, Italia, and IMEM-CNR Institute, 43019, Parma Italia respectively.

1. M.R. Levy, *Tesis Doctoral Departamento de Materiales* (Universidad de Landres, 2005).
2. Y. Romaguerra Barcelay. *Tesis Doctoral en Física* (Universidad de Porto 2012).
3. D. Varshney and N. Kaurav, *Eur. Phys. J. B* **37** (2004) 301-309.
4. S. Ghosh, A.D. Sharma, R.N. Basu, and H.S. Maiti, *J. Am. Ceram. Soc.* **3741** (2007) 3747.
5. F. Fernández. Tesis Doctoral en Química, Universidad de Santiago de Compostela, 2000.
6. E. Pérez, *Seminario, Métodos de Preparación de nanopartículas* (Universidad de los Andes, Mérida Venezuela, 2012).
7. Z.A. Munir, J.B. Holt, *J. Mater. Sci.* **22** (1987) 710-714.
8. E. Chinarró. E. Chinarró, B. Moreno, D. Martín, L. Gonzalez, E. Villanueva, D. Guinea y J.R. Jurado, *Bol. Soc. Esp. Ceram. Vol* **44** (2005) 105-112.
9. A. Kumar, A.S. Verma and S.R. Bhardwaj, *The Open Applied Physics Journal* **1** (2008) 11.
10. J. Coey and S. Von Molnar, *Advances in Physics* **48** (1999) 167.
11. K.B. LiK, X.J. Li and K.G. Zhu, *J. Appl. Phys.* **10** (1997) 6943.
12. H. Wang, Z. Zhao, C.-mingXu and J. Liu, *Catalysis Letters* **102**(2005) 5864.
13. A. Giri, A. Makhal, B. Ghosh, A. K. Raychaudhuri and Samir Kumar Pal, *Nanoscale* **2** (2010) 2704-2709.
14. L.G. Wade, *Química Orgánica*. 5 edición, (2005).
15. V. Zakhvalinski, *Physics of LaMnO<sub>(3±δ)</sub> the Solid State* **48** (2012) 2300.
16. F. Pardo, *Journal of Solid State Chemistry* **146** (1999) 418-427.
17. S.V. Trukhanov, *Journal of Low Temperature Physics* **139** (2005) 4734.
18. J. Topferl and J.B. Odenough, *Chemistry. Journal of Solid State* **130** (1997) 117-128.
19. T.I. Arbutova, *Physic Solid State* **50** (2008) 1487-1494.
20. K. Kamata, *Mat. Res. Bull. Vol.* **13** (1978) 49-54.
21. N. Kamegashira, *Materials Chemistry and Physics* **II** (1984) 181-194.
22. S. Roy, I.S. Dubenko, M. Khan, E.M. Condon, J. Craig, and N. Ali, *Phys. Rev B* **71** (2005) 024419.